Luminous [O III] and [N II] from Tidally Disrupted Horizontal Branch Stars

Drew Clausen – Pennsylvania State University
Steinn Sigurdsson – Pennsylvania State University
Michael Eracleous – Pennsylvania State University
Jimmy A. Irwin – University of Alabama

Citation of published version:

Clausen, D., Sigurdsson, S., Eracleous, M., Irwin, J. (2012): Luminous [O III] and [N II] from Tidally Disrupted Horizontal Branch Stars. *Monthly Notices of the Royal Astronomical Society*, 424(2). DOI: https://doi.org/10.1111/j.1365-2966.2012.21305.x

Monthly Notices
of the
ROYAL ASTRONOMICAL SOCIETY

Mon. Not. R. Astron. Soc. **424,** 1268–1274 (2012) doi:10.1111/j.1365-2966.2012.21305.x

Luminous [O III] and [N II] from tidally disrupted horizontal branch stars

Drew Clausen,[1]★ Steinn Sigurdsson,[1] Michael Eracleous[1] and Jimmy A. Irwin[2]

[1]*Department of Astronomy & Astrophysics, The Pennsylvania State University, 525 Davey Lab, University Park, PA 16802, USA*
[2]*Department of Physics and Astronomy, University of Alabama, Box 870324, Tuscaloosa, AL 35487, USA*

Accepted 2012 May 14. Received 2012 May 11; in original form 2012 April 20

ABSTRACT

We model the emission lines generated in the photoionized debris of a tidally disrupted horizontal branch (HB) star. We find that at late times, the brightest optical emission lines are [N II] λλ6548, 6583 and [O III] λλ4959, 5007. Models of a red clump HB star undergoing mild disruption by a massive (50–100 $M_{\odot}$) black hole (BH) yield an emission-line spectrum that is in good agreement with that observed in the NGC 1399 globular cluster hosting the ultraluminous X-ray source CXOJ033831.8−352604. We make predictions for the ultraviolet emission-line spectrum that can verify the tidal disruption scenario and constrain the mass of the BH.

Key words: black hole physics – globular clusters: general – galaxies: individual: NGC 1399.

1 INTRODUCTION

With the exquisite angular resolution of the *Chandra*, it is possible to resolve low-mass X-ray binaries (LMXBs) in nearby galaxies and to associate these LMXBs with globular clusters (GCs; e.g. Sarazin, Irwin & Bregman 2000). This capability has enabled the discovery of several black hole (BH) candidates in GCs outside of the Milky Way. Maccarone et al. (2007) presented the first strong candidate for a BH in a GC, an ultraluminous X-ray (ULX) source in the GC RZ 2109 associated with the elliptical galaxy NGC 4472. The object's X-ray luminosity of $L_{\rm X} = 4 \times 10^{39}$erg s^{-1} is too large to be explained by accretion on to a neutron star (NS), and the source's strong variability rules out the possibility of a superposition of multiple NSs. Subsequently, three additional ULXs have been identified as GC BH candidates on the basis of their strong X-ray variability: one in NGC 1399 (Shih et al. 2010), one in NGC 3379 (Brassington et al. 2010) and a second candidate in NGC 4472 (Maccarone et al. 2011). Variable X-ray sources with luminosities above the Eddington limit of an NS offer the least ambiguous evidence of a BH accretor; however, Barnard et al. (2011) argued for BH accretors in three LMXBs located in M31 GCs that exhibit low/hard-state spectra at luminosities near an NS's Eddington limit, and in a high-luminosity recurrent transient in a fourth M31 GC.

Irwin et al. (2010, hereafter I10) discussed an additional BH candidate in an NGC 1399 GC; however, the nature of this source is not as clear-cut as that of the other candidates. The object's X-ray luminosity, $L_{\rm X} \sim 2 \times 10^{39}$ erg s^{-1}, suggests a BH accretor, but the 35 per cent decline in the luminosity between 2000 and 2008 does not convincingly rule out a superposition of sources. The X-ray spectrum can be fitted with a power law of photon index $\Gamma = 2.5$, which is much softer than the slope of the power law used to fit the sum of low $L_{\rm X}$ LMXBs ($\Gamma \sim 1.6$). This is also slightly softer than the spectra of other sources with $L_{\rm X} \sim 10^{39}$ erg s^{-1}, which might indicate the presence of a more massive BH. Adding to the intrigue, optical spectroscopy of the NGC 1399 GC revealed bright [N II] λλ6548, 6583 and [O III] λλ4959, 5007 emission lines with luminosities $\sim 10^{36}$ erg s^{-1}, but no Balmer emission lines. This is not the only GC BH with optical emission lines; Zepf et al. (2008) found bright, broad [O III] λ5007 emission lines without accompanying Balmer lines in the optical spectrum of RZ 2109. I10 argued that these two sources could be evidence of the tidal disruption or detonation of a white dwarf by an intermediate-mass BH, based on the lack of hydrogen emission lines in the spectra.

A BH in the core of a galaxy or a GC can tidally disrupt stars that pass too closely, and then accrete a portion of the debris (Hills 1975; Frank & Rees 1976; Sigurdsson & Rees 1997; Baumgardt, Makino & Ebisuzaki 2004; Ramirez-Ruiz & Rosswog 2009). For stars initially on parabolic orbits with the BH, roughly half of the mass of the disrupted star will become bound to the BH, and the other half will remain unbound and stream back out into the cluster (Lacy, Townes & Hollenbach 1982; Rees 1988). Roos (1992) first considered the emission lines produced when the unbound debris is photoionized by the ultraviolet (UV)/X-ray emission generated when the bound portion accretes on to the BH. Detailed studies of the emission lines produced when a main-sequence star is tidally disrupted by a supermassive BH have been made using numerical (Bogdanović et al. 2004) and analytic (Strubbe & Quataert 2009, 2011) models for the dynamical evolution of the debris. Clausen & Eracleous (2011) considered the case of a white dwarf being tidally disrupted by an intermediate-mass BH and found that the emission lines observed in the two BH candidates described above were not consistent with those expected from a tidally disrupted white dwarf. I10 reported that the [N II] and [O III] doublets observed in the NGC 1399 GC have roughly the same luminosity, but the models predict that the [N II] doublet should be two orders of magnitude

★E-mail: dclausen@astro.psu.edu

fainter than the [O III] doublet. The white dwarf tidal disruption models predict that the [O III] λ5007 luminosity will reach a peak value consistent with that observed in RZ 2109 a few years after tidal disruption. However, the X-ray source in RZ 2109 was detected with *ROSAT* in 1994 (Colbert & Ptak 2002), which indicates that the observations reported in Zepf et al. (2008) were made more than a decade after the BH began accreting.

Other models have been proposed to explain the emission lines observed in GCs hosting BH candidates. Maccarone et al. (2010) found that the X-ray emission from RZ 2109 had varied by a factor of 20 over a period of 6 yr, a time-scale far too short to be consistent with a tidal disruption, and suggested that the source is a hierarchical triple system with an inner BH-white dwarf binary. Such a system is in line with the work of Ivanova et al. (2010), who suggested that a triple system may be necessary to form a BH-white dwarf binary. Ripamonti & Mapelli (2012) showed that nova ejecta that have been photoionized by a ULX could produce bright, broad [O III] emission lines similar to those observed in RZ 2109. Porter (2010) considered an accretion disc origin for the emission lines in RZ 2109 and the GC in NGC 1399. Maccarone & Warner (2011) argued that the lines observed in the NGC 1399 GC were formed in the photoionized winds of R Corona Borealis (RCB) stars. Here we propose that the X-ray continuum and optical emission lines observed in the NGC 1399 are the result of a tidal disruption of a horizontal branch (HB) star. In Section 2, we describe the ingredients of our models, in Section 3 we describe the results of our calculations, and in Section 4 we compare our model with competing ones and discuss an observational test to distinguish between them.

2 MODELS

We modelled the emission-line spectrum produced when an HB star on an unbound orbit is disrupted by a BH, using the method outlined in Clausen & Eracleous (2011), which is an adaptation of the procedure used by Strubbe & Quataert (2009). Our approach combines analytic prescriptions for the dynamical evolution of the debris with CLOUDY (Ferland et al. 1998) photoionization models to compute the luminosities and line profiles of the emission lines produced in the unbound portion of the debris. These models require as inputs the mass of the disrupted star $M_\star$, the radius of the disrupted star $R_\star$, the mass of the BH $M_{\rm BH}$, the pericentre distance of the orbit $R_{\rm P}$ and the composition of the disrupted star. We determined the properties of the HB stars used in our models using the stellar evolution code MESA STAR (Paxton et al. 2011).

2.1 HB star models

A GC's HB morphology is strongly influenced by its metallicity, with the HBs in most metal-rich GCs lying redwards of the instability strip and those of most low-metallicity clusters lying to the blue side. However, it has been known for some time that metallicity alone cannot account for the range of HB morphologies observed, and that HB morphology is determined by metallicity and at least a second parameter (e.g. Sandage & Wallerstein 1960; van den Bergh 1967). By the mid-1990s, a number of studies (e.g. Searle & Zinn 1978; Lee, Demarque & Zinn 1994) had established cluster age as a likely solution to the second parameter problem. Recent, independent studies by Dotter et al. (2010) and Gratton et al. (2010) have confirmed that the second parameter is the age of the GC. The GC hosting the X-ray source considered here is quite red ($B - I = 2.25$; Kundu, Maccarone & Zepf 2007), and therefore likely has a HB consisting primarily of red clump stars, which is typical of high metallically GCs. However, there is evidence that some metal-rich GCs harbour extreme horizontal branch (EHB) and even blue hook stars (e.g. Rey et al. 2007; Dalessandro et al. 2008; Peacock et al. 2010), so we will consider the tidal disruption of both red clump and EHB stars.

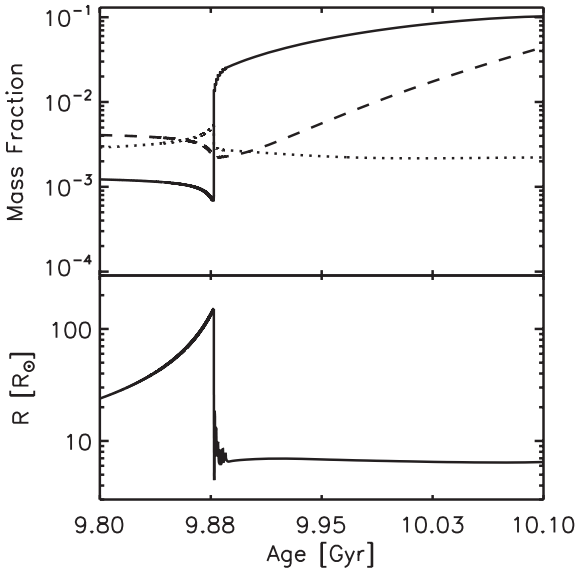

Figure 1. Mass fractions (top) of carbon (solid), nitrogen (dotted) and oxygen (dashed) versus time and radius (bottom) versus time from the MESA STAR model of a 1 $M_\odot$ star with $Z = Z_\odot/2$.

Using MESA STAR, we evolved a $1\,M_\odot$ star with $Z = Z_\odot/2$ to determine the mass, radius and composition of the red clump star. The star evolved to the HB after ∼9.9 Gyr, at which point $M_\star = 0.67\,M_\odot$ and $R_\star = 6.2\,R_\odot$ (see Fig. 1). Furthermore, CNO cycle burning had enriched the core of the star with nitrogen at the expense of carbon and oxygen. Leading up to the HB phase, the total mass fraction of nitrogen rose and those of oxygen and carbon fell as the star's relatively carbon and oxygen rich envelope was shed. The ratio of nitrogen to oxygen is highest right after helium ignition, at the start of the HB phase. We used the mass, radius and composition of the HB star at this point as our fiducial model. At this point, the star was made up of 15 per cent H, 84 per cent He, 0.1 per cent C, 0.5 per cent N and 0.2 per cent O, by mass, with all other elements present in their initial mass fraction. The mass and radius of our adopted HB star is consistent with previous models (e.g. Dorman 1992; Charbonnel et al. 1996). Furthermore, measurements of the surface abundances in HB stars have revealed a nitrogen enhancement, but the surface abundance of nitrogen, which depends on a star's mixing history, is highly variable from star to star (e.g. Behr et al. 1999; Gratton et al. 2000; Tautvaišienė et al. 2001).

We found $M_\star = 0.49\,M_\odot$ and $R_\star = 0.12\,R_\odot$ for an EHB star by running a MESA STAR model of a $1\,M_\odot$ star with $Z = 0.1\,Z_\odot$. This combination of $M_\star$ and $R_\star$ are in good agreement with the asteroseismology measurements of the masses and radii of hot subdwarfs (Charpinet et al. 2008; van Grootel et al. 2010). The composition of the EHB star was 5.2 per cent H, 94.5 per cent He, 5×10^{-3} per cent C, 0.1 per cent N and 0.03 per cent O.

2.2 Tidal disruption models

Here we briefly describe our tidal disruption models, and we refer the reader to Clausen & Eracleous (2011) and Strubbe & Quataert (2009) for a complete description. We assume that the HB star is on a

parabolic orbit with $R_P \leq R_T$, where R_T is the tidal disruption radius, $R_T = R_\star(M_{BH}/R_\star)^{1/3}$. The strength of the encounter is set with the tidal disruption parameter $\beta = R_T/R_P$. After tidal disruption, half of the disrupted star falls back to the BH and forms a thin accretion disc. The rate at which material falls back declines with time as $\dot{M} \propto t^{-5/3}$. When $\dot{M}$ exceeds the BH's Eddington rate, we assume that the excess is driven away in an outflow but we do not include the outflowing material in our models (see Strubbe & Quataert 2011 for an exploration of the outflow). This results in the accretion flare having a constant luminosity of $L = 1.3 \times 10^{38}\, M_{BH}\, \mathrm{erg\,s^{-1}}$ during this super-Eddington phase.

The other half of the debris remains unbound and moves away from the BH with a range of velocities given by $v(\phi) = (2GM_{BH}/R_P)^{1/2}\cot(\phi/2)$, where ϕ is the azimuthal angle in the orbital plane and is in the range $(\pi - (12R_\star/R_P)^{1/2}) < \phi < \pi$. The density in the debris tail is given by $n(\phi, t) = n_0[v(\phi)t]^{-3}$, where t is the time since tidal disruption and the normalization factor n_0 is set such that the total mass in the debris tail is $M_\star/2$. We divide the debris tail into six azimuthal zones and compute photoionization models for each zone with version 10.00 of CLOUDY (Ferland et al. 1998), using the density determined by the dynamical model and the composition given by the MESA STAR models. The spectral energy distribution (SED) and intensity of the ionizing radiation are determined from the dynamical model of the bound debris. We assume a standard α-disc model with $\alpha = 0.1$, an inner radius of three times Schwarzschild radius, an outer radius of $2R_P$ and mass accretion rate equal to the mass fallback rate described above. Using the range of temperatures in the accretion disc, we construct a multicolour blackbody which we use as the ionizing continuum for the CLOUDY models. We have not added an X-ray power law to the SEDs used in these models. Photoionization by X-rays can result in significant heating of the unbound material and affect the luminosities of collisionally excited emission lines. However, Clausen & Eracleous (2011) found that the luminosities of the optical emission lines of interest here were not sensitive to this additional component.

We modelled the emission lines produced with 20 different sets of initial conditions to explore the parameter space in BH mass ($30\,M_\odot \leq M_{BH} \leq 10^4\,M_\odot$), HB star structure and composition (red clump and EHB), and tidal disruption parameter β ($0.1 \leq \beta \leq 1$).

3 RESULTS

Each combination of M_{BH}, HB star type and β that we considered predicted [N II] λ6583 and [O III] λ5007 emission lines with luminosities $\sim 10^{36}\,\mathrm{erg\,s^{-1}}$ at some point during the post-tidal-disruption evolution. However, only those with a red clump HB star, a BH with $M_{BH} \lesssim 200\,M_\odot$ and $\beta \sim 1$ were able to reproduce the emission-line luminosity ratios reported in I10. These constraints are [N II] λ6583/Hα > 7, [O III] λ5007/Hβ > 5 and [N II] λ6583/[O III] λ5007 ∼ 1. We plot the time evolution of these ratios for a subset of our models in Fig. 2. In the models plotted here, we have used our fiducial red clump HB star and assumed that $R_P = R_T$, but varied M_{BH}.

In each of these models, the Balmer lines outshone the [O III] and [N II] lines initially. Then, as the debris cloud expanded and n decreased, the luminosity of the Balmer lines declined because the volume emissivity of these permitted transitions is proportional to the product of the electron and ionized hydrogen number densities. At the same time, the [O III] λ5007 and [N II] λ6583 lines became brighter. These forbidden lines are produced when ions are collisionally excited into a metastable state and then de-excite radiatively. As the density in the unbound debris decreased, the collision rate declined, allowing a larger fraction of the excited ions to decay radiatively, as opposed to collisionally, and the forbidden emission lines grew brighter. As a result, all of the models shown in Fig. 2 can satisfy the [O III]/Hβ constraint, provided we are observing the debris more than 40 yr after tidal disruption. The models with $M_{BH} = 10^3$ and $10^4\,M_\odot$ were unable to reproduce the observed [N II]/Hα ratio. These more massive BHs permit higher accretion rates that led to an increased flux of ionizing photons. By the time the density in the debris was low enough to produce a significant [N II] luminosity, [N II] emission was suppressed because the cloud had become so highly ionized that much of the N^+ was further ionized to N^{++}.

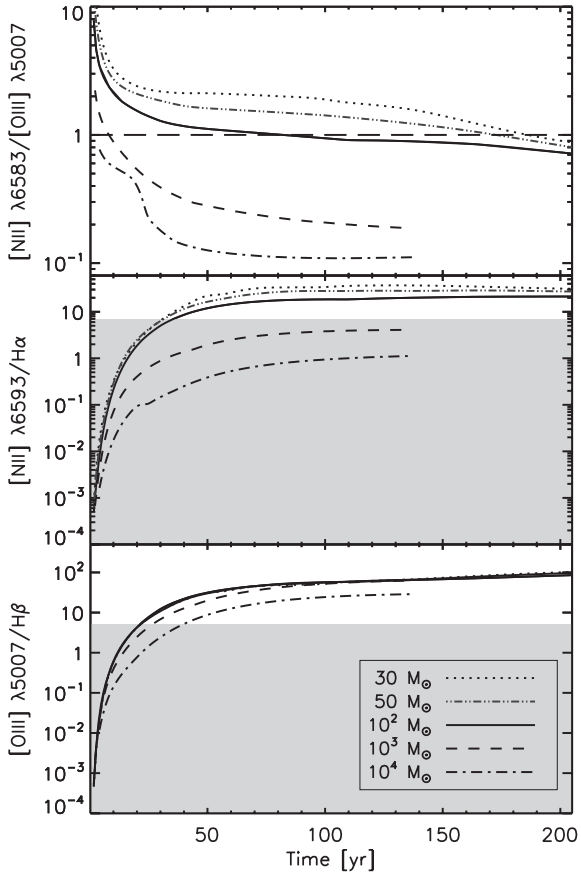

Figure 2. Emission-line luminosity ratios over time from several tidal disruption models with varying M_{BH}. The long dashed line in the top panel shows the constraint on the [N II]/[O III] ratio measured by I10. Models that fall near this line are consistent with the observations. In the lower two panels, the shaded region indicates line ratios ruled out by the observations of I10; only models that reach into the unshaded region are consistent with the observations. For each model shown here, we considered a red clump star on an orbit with $R_P = R_T$.

This over-ionization of the unbound debris also drove the evolution of the [N II]/[O III] ratio. In all of the models, the ratio steadily declined as an increasing portion of the oxygen and nitrogen in the cloud became doubly ionized. With $M_{BH} = 10^3$ or $10^4\,M_\odot$, the unbound debris became too highly ionized for the [N II]/[O III] ratio to be ∼1 within 10 yr of tidal disruption (see Fig. 2). We found that in models with $M_{BH} < 200\,M_\odot$, the decline is slow enough that the luminosities of the two forbidden emission lines can differ by less than a factor of 2 for up to 200 yr.

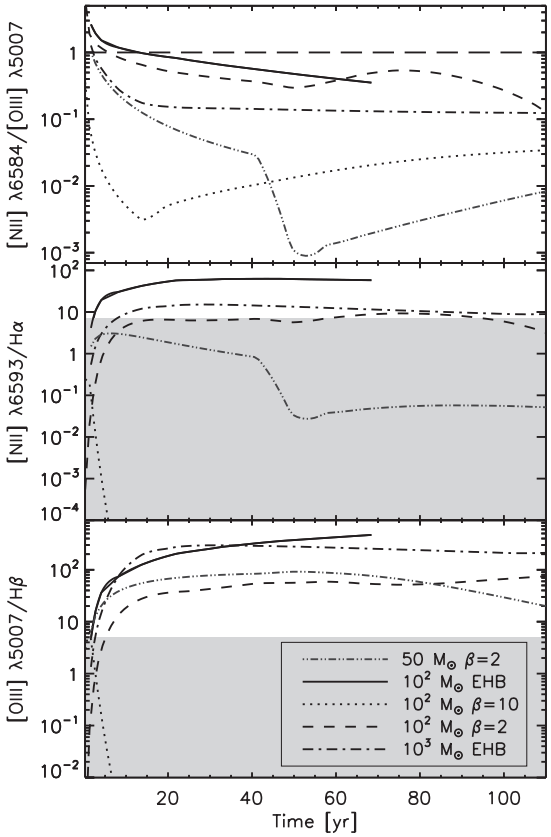

Figure 3. Emission-line luminosity ratios over time from several tidal disruption models with varying $M_{\rm BH}$, tidal disruption parameter β and stellar type. The long dashed line in the top panel shows the constraint on the [N II]/[O III] ratio measured by I10. Models that fall near this line are consistent with the observations. In the lower two panels, the shaded region indicates line ratios ruled out by the observations of I10; only models that reach into the unshaded region are consistent with the observations.

Fig. 3 shows a number of alternative models for strong disruption and/or blue HB stars. These models fail to reproduce the observed [N II]/[O III] ratio for an extended period of time, in contrast to our models of weakly disrupted red HB stars. Like the models involving high-mass BHs discussed above, the unbound debris cloud becomes too highly ionized to produce significant [N II] emission. Using a simple estimate of the ionization parameter $U = n_\gamma/n_{\rm H}$, we can illustrate why some debris clouds become over-ionized and others do not. Here n_γ is the number density of photons with energies above 13.6 eV and $n_{\rm H}$ is the hydrogen number density. Recasting the ionization parameter in terms of our model parameters, we find $U \propto R_\star^{-1/2}\beta^3\dot{M}^{3/4}t$. Debris from stars with a larger kinetic energy at pericentre passage, due to a more compact star with smaller $R_{\rm T}$, an orbit with $\beta > 1$ or a more massive BH, spanned a wider range in velocity and quickly expanded to a low density, resulting in a large U. As mentioned above, more massive BHs led to a higher flux of ionizing photons, also contributing to increased U. During the super-Eddington phase, $\dot{M} \propto M_{\rm BH}$ was constant and the ionization parameter increased with time. The N^+ fraction reached a maximum[1] when $U \sim 0.06$, and at larger values of U, the luminosity of the [N II] line declined. Keeping the ionization state in the unbound debris low enough to produce significant [N II] emission after the super-Eddington phase had ended required the relatively large radius of the red clump star and a BH of relatively low mass, $M_{\rm BH} < 200\,{\rm M}_\odot$. After the super-Eddington phase, U declined as $t^{-1/4}$ and N^{++} recombined into N^+. This drove the [N II]/[O III] ratio back towards unity in some cases (see models with $\beta > 1$ in Fig. 3). However, at this point the density in the cloud is so low that the luminosities of the lines are well below the observed values.

[1] The value of U at which this maximum occurs is abundance dependent. The value given is for the red clump star composition. The maximum occurs at a much smaller value of U if solar abundances are used.

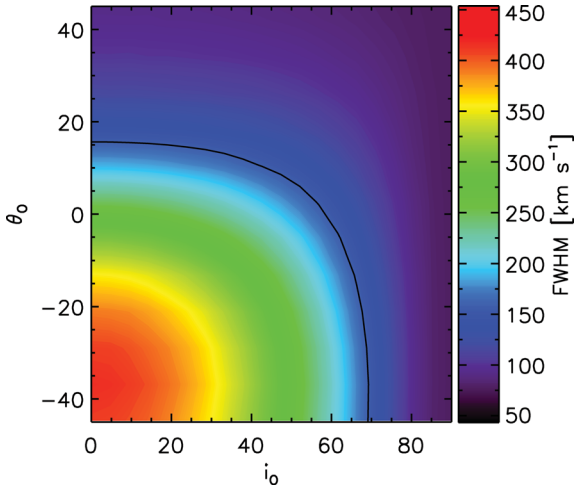

Figure 4. FWHM of the [N II] λ6583 emission line 125 yr after tidal disruption, synthesized from a model using the red clump star, $\beta = 1$, and $M_{\rm BH} = 100\,{\rm M}_\odot$. The angles θ_0 and i_0 describe the orientation of the observer (see fig. 1 in Clausen & Eracleous 2011). The black curve marks the observed FWHM. Any pair of θ_0 and i_0 along the black line produces a FWHM that is consistent with observations.

Finally, by combining the dynamical model with the photoionization model, we synthesized the emission-line profiles of the [N II] and [O III] lines. Fig. 4 shows the range of observed full width at half-maximum (FWHM) of the [N II] line produced in the model of a red clump star on an orbit with $\beta = 1$ being tidally disrupted by a $100\,{\rm M}_\odot$ BH, 125 yr after tidal disruption. The angles θ_0 and i_0 describe the orientation of the observer and are the angle between the line of site and the direction of pericentre and the orbital plane, respectively. The black line shows the observed FWHM = 140 km s^{-1}. For a range of observer orientations, the FWHM of the synthesized emission lines is consistent with the observations.

4 DISCUSSION

We have shown that the photoionized debris of a tidally disrupted HB star can account for the emission lines observed in optical spectra presented in I10. Reproducing the line ratios within the context of this model requires $M_{\rm BH} \lesssim 200\,{\rm M}_\odot$. In these scenarios, the super-Eddington phase lasts between 90 and 155 yr. Since we have not included the outflow produced during this phase in our models, the emission-line luminosities calculated during this period are uncertain. However, the modelled emission-line luminosities remain consistent with the observations after the super-Eddington phase has ended. Furthermore, the X-ray luminosity of the accretion flare does not decline to the observed value of $L_{\rm X} \sim 2 \times 10^{39}$ erg s^{-1} until after the mass fall back rate has dropped below the Eddington rate. Archival images taken with the *ROSAT* High Resolution Imager establish that the X-ray source has been on since at least 1996 January. At times greater than $t = 200$ yr after disruption, our assumption

of steady state accretion begins to break down because the viscous time in the accretion disc approaches t. We have also checked that the conditions in the photoionized debris change slowly enough that the unbound debris remained in photoionization equilibrium for the entire period explored in our models.

We did not consider spinning BHs in this study. The last stable orbit around a spinning BH is closer to the event horizon, allowing the accretion disc to extend to smaller radii than the discs considered here. Accretion discs around spinning BHs produce a larger flux of ionizing photons with an SED that peaks at a higher photon energy because the maximum temperature in these discs is larger than that of accretion discs around non-spinning BHs. However, unlike the supermassive BHs found in the cores of galaxies, BHs in GCs have not gained an appreciable portion of their mass though disc accretion. Belczynski et al. (2008) found that any accretion that does occur while the BH is in a mass transferring binary does not substantially increase its spin. However, it is possible that the GC BHs are born with a large spin. If this is the case, the HB tidal disruption scenario remains a plausible explanation for the observed emission lines, but the BH mass inferred from the models would change by a factor of a few.

The [N II]/[O III] ratio is sensitive to the abundance of nitrogen and oxygen in the HB star. In the models discussed above, we used the composition of the HB star at the onset of helium burning, when the ratio of nitrogen to oxygen is largest. Helium burning destroys nitrogen and creates oxygen, so N/O declines as the star evolves on the HB. Fig. 5 shows how [N II]/[O III] responds to changes in composition of the HB star. In these models, we used the composition of the red clump star at later times, as computed in the MESA STAR models, corresponding to points where the nitrogen and oxygen abundances are equal, and where the nitrogen abundance is half that of oxygen. The mass and radius of the star did not change appreciably in this time, so we used the same values as in our fiducial model, and we used $\beta = 1$. When $M_{\rm BH} = 50\,{\rm M}_{\odot}$, the models with both abundance sets are consistent with the observed [N II]/[O III]. The [N II]/[O III] ratio drops too quickly to be consistent with observations when $M_{\rm BH} = 100\,{\rm M}_{\odot}$ and the oxygen abundance is twice that of nitrogen. This sets the period during which the HB star can be disrupted by the BH and produce the observed emission-line spectrum. For the $100\,{\rm M}_{\odot}$ BH, the HB star must be disrupted within 30 Myr of helium ignition to satisfy the [N II]/[O III] constraint, while a $50\,{\rm M}_{\odot}$ BH can disrupt the HB star within 80 Myr of helium ignition and meet the constraint.

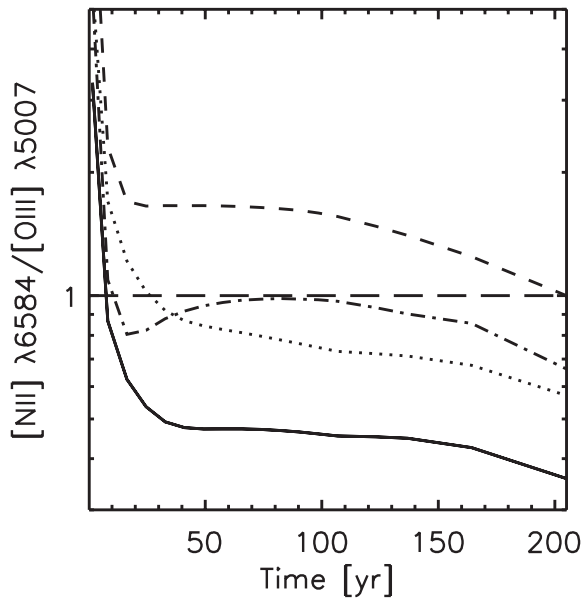

Figure 5. Evolution of [N II]/[O III] for HB stars of different composition. We show two sets of models – young HB stars 30 Myr after He ignition when the nitrogen and oxygen abundance are equal ($M_{\rm BH} = 50\,{\rm M}_{\odot}$, dashed; $M_{\rm BH} = 100\,{\rm M}_{\odot}$, dotted) and the same models but with the HB star older so that 80 Myr of He burning has made oxygen twice as abundant as nitrogen ($M_{\rm BH} = 50\,{\rm M}_{\odot}$, dot–dashed; $M_{\rm BH} = 100\,{\rm M}_{\odot}$, solid). For a $100\,{\rm M}_{\odot}$ BH, the observed [N II]/[O III] ratio cannot be reproduced once helium burning has created an oxygen abundance that is twice the nitrogen abundance.

It is appealing that the tidal disruption models require a red HB star to meet the observational constraints on the emission-line ratios. The host GC is red and likely exhibits the red HB morphology typical of a metal-rich cluster. However, given the predicted rate at which GC BHs tidally disrupt stars, it is surprising that such an event might have been observed. Employing the tidal disruption rate equation computed by Baumgardt et al. (2004), with the mass and radius of a red clump HB star, $M_{\rm BH} = 100\,{\rm M}_{\odot}$, a core density of $5 \times 10^5\,{\rm pc}^{-3}$, a core velocity of $10\,{\rm km\,s}^{-1}$ and assuming that 5 per cent of the stars in a GC's core are HB stars, we find a HB tidal disruption rate of $1.2 \times 10^{-10}\,{\rm yr}^{-1}\,{\rm GC}^{-1}$. Given that the bright [N II] and [O III] emission lines persist for 200 yr, and that the space density of GCs is $\sim$6 Mpc^{-3} (Croton et al. 2005; Brodie & Strader 2006), at any time there should only be 5×10^{-3} observable HB tidal disruptions within the 20 Mpc distance to NGC 1399. Furthermore, if the NGC 1399 GC source is the aftermath of an HB tidal disruption, it is also puzzling that several main-sequence tidal disruptions have not been observed because they should occur more frequently (Baumgardt et al. 2004).

The low disruption rate and the dearth of main-sequence tidal disruptions are only an issue if the tidal disruption occurs through the conventional loss cone orbit channel. One possibility that would result in the preferential disruption of post-main-sequence stars is for the disrupted star to be bound to the BH. If this is the case, tidal disruption could be triggered in two different scenarios: (1) a scattering induced merger or (2) a triple decay. In a scattering-induced merger, the HB star progenitor is bound to the BH, expands to fill its Roche lobe while on the giant branch, and transfers material to the BH. During mass transfer, the semimajor axis of the binary expands, greatly increasing the likelihood that the binary will undergo an encounter with another star in the GC. Such an encounter could impulsively increase the eccentricity and decrease the semimajor axis of the binary and result in the tidal disruption of the bound star (Sigurdsson & Phinney 1993, 1995; Davies 1995). Successive distant encounters can also drive the eccentricity high enough for $R_{\rm P} = R_{\rm T}$. We have estimated the time-scale for this process using the expression given in Maccarone (2005), which uses the encounter cross-sections computed by Heggie & Rasio (1996). In a binary with a post-mass-transfer semimajor axis of 1 au containing a $100\,{\rm M}_{\odot}$ BH, a $0.65\,{\rm M}_{\odot}$ HB star will be driven to the tidal disruption radius in 10 Myr. This is well within the 30 Myr window required to produce [N II] and [O III] emission lines of similar luminosity. Here we have assumed that the field stars have mass $0.8\,{\rm M}_{\odot}$, a cluster density of $5 \times 10^5\,{\rm pc}^{-3}$ and a velocity of dispersion of $10\,{\rm km\,s}^{-1}$. A scattering-induced merger would be more likely in a dense GC.

In the triple decay, the BH and HB star progenitor are initially the inner binary in a stable, hierarchal triple system. Again, the evolution of the HB progenitor results in a phase of mass transfer and expansion of the inner binary's semimajor axis. In this case, expansion of the inner binary drives the triple to instability and triggers the tidal disruption. A similar scenario was discussed by

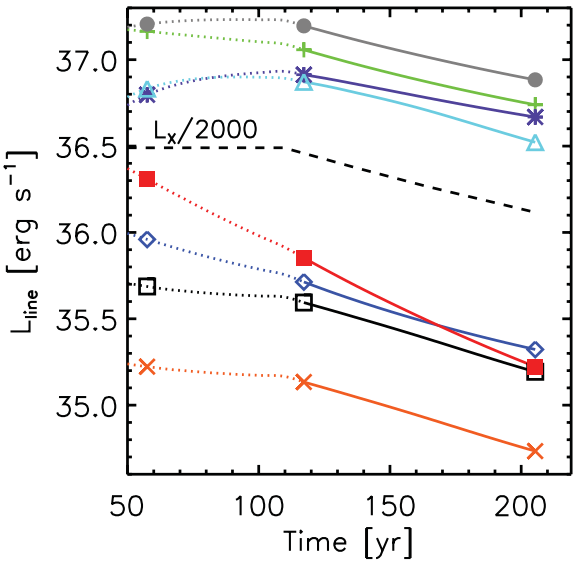

Figure 6. Light curves from a model using the fiducial red clump HB star, $\beta = 1$, and $M_{BH} = 100\,M_{\odot}$. Emission-line light curves are shown for N v λ1240 (grey, filled circle), C iv λ1548 (green, plus), [O iii] λ5007 (purple, asterisk), [N ii] λ6583 (light blue, triangle), N ii λ5755 (red, filled box), O iii λ4363 (dark blue, diamond), Hα (black, open box) and Hβ (orange, x). The dashed curve shows L_X scaled down by a factor of 2000. Note the bright N v and C iv doublets predicted by the model. The dotted portion of each curve shows the line luminosity while the fallback rate is super-Eddington and our model is uncertain.

Perets & Kratter (2012); only these authors invoked mass-loss, not mass transfer, to drive the expansion of the inner binary. The triple decay scenario would require a medium density GC, because triple systems are unstable to external perturbations in dense GCs. Both the scattering-induced merger and triple decay scenarios increase the odds that tidal disruptions are linked to post-main-sequence stars, but determining whether disruption through either scenario would occur more frequently than the loss cone tidal disruptions discussed above is beyond the scope of this paper.

Our models also predict several strong UV emission lines. These lines could be used to test the tidally disrupted HB star hypothesis for the ULX in NGC 1399 and to further constrain the mass of the BH. The strongest lines are N v λλ1239, 1243, O vi λλ1032, 1038, N iv] λ1486 and C iv λλ1548, 1550. These lines should have FWHM similar to the observed optical lines. The bright C iv doublet could be used to constrain the composition of the disrupted star and narrow the allowed range in M_{BH}. The light curves for the N v and C iv emission lines are shown in Fig. 6 along with the emission-line light curves for the optical lines with observational constraints. In contrast, Maccarone & Warner (2011) do not report any strong UV lines from their models of photoionized RCB star winds.

5 CONCLUSION

We have presented models for the emission lines generated in the photoionized debris of tidally disrupted HB stars. Within the assumptions made in our models, the emission-line spectra produced when a red clump star is disrupted by a BH with $M_{BH} \lesssim 200$ are consistent with the optical emission lines observed by I10 in the ULX hosting GC in NGC 1399. The models also make testable predictions about the source's UV emission-line spectrum. Observations of the UV emission lines could significantly improve our understanding of this source and are likely possible with the *Hubble Space Telescope*.

ACKNOWLEDGMENTS

We thank the anonymous referee for a prompt and helpful review. DC is supported by the PSU Academic Computing Fellowship. The authors thank the Aspen Center for Physics for its hospitality.

REFERENCES

Barnard R., Garcia M., Li Z., Primini F., Murray S. S., 2011, ApJ, 734, 79
Baumgardt H., Makino J., Ebisuzaki T., 2004, ApJ, 613, 1143
Behr B. B., Cohen J. G., McCarthy J. K., Djorgovski S. G., 1999, ApJ, 517, L135
Belczynski K., Taam R. E., Rantsiou E., van der Sluys M., 2008, ApJ, 682, 474
Bogdanović T., Eracleous M., Mahadevan S., Sigurdsson S., Laguna P., 2004, ApJ, 610, 707
Brassington N. J. et al., 2010, ApJ, 725, 1805
Brodie J. P., Strader J., 2006, ARA&A, 44, 193
Charbonnel C., Meynet G., Maeder A., Schaerer D., 1996, A&AS, 115, 339
Charpinet S., van Grootel V., Reese D., Fontaine G., Green E. M., Brassard P., Chayer P., 2008, A&A, 489, 377
Clausen D., Eracleous M., 2011, ApJ, 726, 34
Colbert E. J. M., Ptak A. F., 2002, ApJS, 143, 25
Croton D. J. et al., 2005, MNRAS, 356, 1155
Dalessandro E., Lanzoni B., Ferraro F. R., Rood R. T., Milone A., Piotto G., Valenti E., 2008, ApJ, 677, 1069
Davies M. B., 1995, MNRAS, 276, 887
Dorman B., 1992, ApJS, 81, 221
Dotter A. et al., 2010, ApJ, 708, 698
Ferland G. J., Korista K. T., Verner D. A., Ferguson J. W., Kingdon J. B., Verner E. M., 1998, PASP, 110, 761
Frank J., Rees M. J., 1976, MNRAS, 176, 633
Gratton R. G., Sneden C., Carretta E., Bragaglia A., 2000, A&A, 354, 169
Gratton R. G., Carretta E., Bragaglia A., Lucatello S., D'Orazi V., 2010, A&A, 517, A81
Heggie D. C., Rasio F. A., 1996, MNRAS, 282, 1064
Hills J. G., 1975, Nat, 254, 295
Irwin J. A., Brink T. G., Bregman J. N., Roberts T. P., 2010, ApJ, 712, L1 (I10)
Ivanova N., Chaichenets S., Fregeau J., Heinke C. O., Lombardi J. C., Jr, Woods T. E., 2010, ApJ, 717, 948
Kundu A., Maccarone T. J., Zepf S. E., 2007, ApJ, 662, 525
Lacy J. H., Townes C. H., Hollenbach D. J., 1982, ApJ, 262, 120
Lee Y.-W., Demarque P., Zinn R., 1994, ApJ, 423, 248
Maccarone T. J., 2005, MNRAS, 364, 971
Maccarone T. J., Warner B., 2011, MNRAS, 410, L32
Maccarone T. J., Kundu A., Zepf S. E., Rhode K. L., 2007, Nat, 445, 183
Maccarone T. J., Kundu A., Zepf S. E., Rhode K. L., 2010, MNRAS, 409, L84
Maccarone T. J., Kundu A., Zepf S. E., Rhode K. L., 2011, MNRAS, 410, 1655
Paxton B., Bildsten L., Dotter A., Herwig F., Lesaffre P., Timmes F., 2011, ApJS, 192, 3
Peacock M. B., Maccarone T. J., Knigge C., Kundu A., Waters C. Z., Zepf S. E., Zurek D. R., 2010, MNRAS, 402, 803
Perets H. B., Kratter K. M., 2012, preprint (arXiv:1203.2914)
Porter R. L., 2010, MNRAS, 407, L59
Ramirez-Ruiz E., Rosswog S., 2009, ApJ, 697, L77
Rees M. J., 1988, Nat, 333, 523
Rey S. C. et al., 2007, ApJS, 173, 643
Ripamonti E., Mapelli M., 2012, MNRAS, 423, 1144
Roos N., 1992, ApJ, 385, 108
Sandage A., Wallerstein G., 1960, ApJ, 131, 598
Sarazin C. L., Irwin J. A., Bregman J. N., 2000, ApJ, 544, L101

Searle L., Zinn R., 1978, ApJ, 225, 357
Shih I. C., Kundu A., Maccarone T. J., Zepf S. E., Joseph T. D., 2010, ApJ, 721, 323
Sigurdsson S., Phinney E. S., 1993, ApJ, 415, 631
Sigurdsson S., Phinney E. S., 1995, ApJ, 99, 609
Sigurdsson S., Rees M. J., 1997, MNRAS, 284, 318
Strubbe L. E., Quataert E., 2009, MNRAS, 400, 2070
Strubbe L. E., Quataert E., 2011, MNRAS, 415, 168
Tautvaišienė G., Edvardsson B., Tuominen I., Ilyin I., 2001, A&A, 380, 578
van den Bergh S., 1967, AJ, 72, 70
van Grootel V., Charpinet S., Fontaine G., Green E. M., Brassard P., 2010, A&A, 524, A63
Zepf S. E. et al., 2008, ApJ, 683, L139

This paper has been typeset from a TEX/LATEX file prepared by the author.